Finite-Difference Time-Domain Approach to Underwater Acoustic Scattering Problems

Shuozhong Wang

Shanghai University, Shanghai 200072, China

The finite-difference time-domain (FDTD) recurrence expressions are formulated, and the numerical algorithm developed for underwater acoustic scattering applications, based upon the basic motion equation and the equation of continuity. The boundary condition implementation for both soft and rigid surfaces, and the absorbing boundary conditions on the truncating surface are described. The algorithm simulates the sound wave propagation in the time domain. As the time-stepping proceeds, boundary conditions are satisfied naturally. The method is particularly suited for scattering from complex objects. Near-field distributions of waves scattered from cylinders with ideal boundary conditions, insonified by a plane incident wave, are first computed. Far-field directional patterns are then derived using a Fourier transform method. The method is then applied to some other objects, including a square cylinder with an arbitrary aspect angle, and wedges with either ideally soft or ideally rigid surfaces. A good agreement between the FDTD and the theoretical results is demonstrated, showing the potential of the method in the studies of underwater scattering problems.

PACS numbers: 43.30.Gv, 43.30.Es, 43.20.Fn

INTRODUCTION

Since its introduction by Yee in 1966[1], the finite-difference time-domain (FDTD) method has been used extensively in electromagnetism. The method involves discretization of the Maxwell's time dependent curl equations and simulation of wave propagation in the time domain. A set of explicit expressions are obtained from the first order difference equations in a form suitable for numerical computation. The FDTD concept is simple and straightforward, yet remarkably effective and accurate for a wide range of applications, including studies on antenna characteristics[2], transient field phenomena[3], interaction of EM waves with objects[4], prediction of radar cross-sections (RCS)[5], etc. With the recent advances of computer technology, FDTD is attracting even more attention in various areas of the EM theory and its practical aspects.

Applications of numerical solutions of time dependent partial differential equations using finite difference modeling can also be found in other fields, such as geoacoustics and seismology[6,7,8], fluid dynamics[9], etc. Some of these studies discussed elastic and compression waves in both homogeneous and heterogeneous media, associated with seismological phenomena. In underwater acoustics, J. A. Clark et al.[10] described a method using finite difference approximation of the Helmholtz integral equation to obtain the radiated field distribution from measurements around an immersed structure. J. R. Fricke[11] studied acoustic scattering from Arctic ice features. In his work, the quasilinear elastodynamic equations are solved using a Lax-Wendroff conservation law finite difference scheme. R. A. Stephen[12] reviewed a number of finite difference methods based on discretization of the second order wave equation for their applicability in dealing with seismic wave propagation in seafloor environments.

In this paper, we demonstrate the usefulness of the FDTD method in solving underwater acoustic problems, and in particular, scattering problems. The FDTD expressions are first formulated based on the basic motion equation and continuity equation, rather than the second order wave equation as in the seismological work mention above. This is followed by a discussion of the implementation of acoustic boundary conditions for ideally soft and rigid objects, and the absorbing boundary conditions on the outer boundary of the region. The acoustic field is simulated in the time domain, starting from an initial state where a plane wave is propagated into the region of concern; and the wave front is about to encounter an object. The wave is then scattered by the object as it advances; and the boundary conditions are satisfied in a natural way. The algorithm gives the instantaneous distribution of the field parameters. A typical case in which plane waves are scattered by a circular cylinder with ideal boundary properties is first studied in order to verify the computer algorithm. The near-field scattered wave is computed; and from it, the far-field directional pattern derived. The pattern is compared with the theoretical results obtained from a classic analytical solution. Some other examples are then given. These include field patterns of scattered waves by a rectangular cylinder with an arbitrary aspect angle, and by wedges with an arbitrary interior angle, both soft and rigid. The results of wedge diffraction are also compared with theoretical results. These have shown the potential scope of applications of the method in studying underwater acoustic scattering from complex objects.

I. FDTD FORMULATION IN ACOUSTICS

A. Basic difference expressions

Consider sound waves propagating in the water. In stead of the wave equation, we base our work on the basic Euler's equation and the equation of continuity. For simplicity, the discussion is confined to a two-dimensional space. Generalization to three-dimension should be straightforward. In a 2-D Cartesian coordinate system, the sound pressure p and the particle velocity $\mathbf{u}$ satisfy the following equations:

$$\frac{\partial p}{\partial x} = -\rho \frac{\partial u_x}{\partial t} , \tag{1}$$

$$\frac{\partial p}{\partial y} = -\rho \frac{\partial u_y}{\partial t} , \tag{2}$$

$$\frac{\partial u}{\partial x} + \frac{\partial u}{\partial y} = -\frac{1}{\rho c^2} \frac{\partial p}{\partial t} , \tag{3}$$

where ρ is the density of the medium, and c is the sound speed.

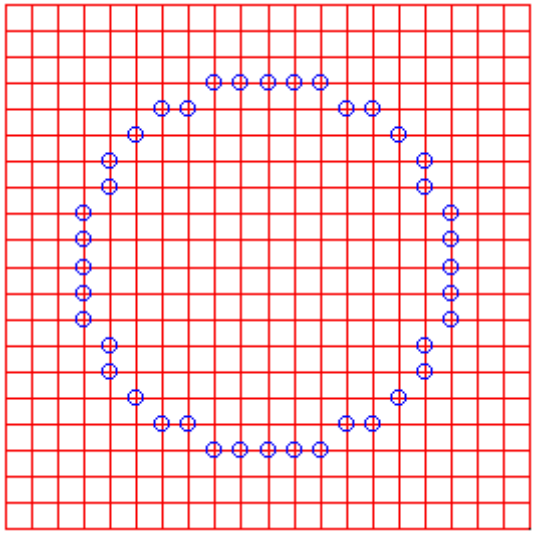

Figure 1 Lattice structure: boundary locations are approximated to the nearest lattice points.

To derive the finite difference form of these partial differential equations, both time and space need to be discretized. In the space, a square lattice with a grid size of δ is chosen. Any boundary locations are approximated to the nearest lattice points, as shown in Figure 1. The lattice spacing δ should be sufficiently small, generally one tenth of the wavelength or less, to give an adequate space sampling. Therefore the first-order partial derivatives of a field parameter $f(x, y; t)$ with respect to x and y can be approximated as the following central differences:

$$\frac{\partial f(x,y;t)}{\partial x} \to \frac{1}{2\delta} \left[f^{(n)}(i+1, j) - f^{(n)}(i-1, j) \right] , \tag{4}$$

$$\frac{\partial f(x,y;t)}{\partial y} \to \frac{1}{2\delta} \left[f^{(n)}(i, j+1) - f^{(n)}(i, j-1) \right] . \tag{5}$$

Central differences provide second-order accuracy compared to biased differences. Similarly, the partial derivative of $f(x, y; t)$ with respect to t can be approximated as

$$\frac{\partial f(x,y;t)}{\partial t} \to \frac{1}{2\Delta t} \left[f^{(n+1)}(i, j) - f^{(n-1)}(i, j) \right] . \tag{6}$$

Here we follow Yee's notations where i and j are the spatial indices representing discretized x and y respectively, and n is the temporal index. Substituting these difference expressions into Eqs. (1) – (3), the following recurrence relations are obtained:

$$u_x^{(n)}(i, j) = u_x^{(n-2)}(i, j) - \frac{\Delta t}{\delta \rho} \left[p^{(n-1)}(i + 1, j) - p^{(n-1)}(i - 1, j) \right], \tag{7}$$

$$u_y^{(n)}(i, j) = u_y^{(n-2)}(i, j) - \frac{\Delta t}{\delta \rho} \left[p^{(n-1)}(i, j + 1) - p^{(n-1)}(i, j - 1) \right], \tag{8}$$

$$p^{(n)}(i, j) = p^{(n-2)}(i, j) - \frac{\rho c^2 \Delta t}{\delta} \left[u_x^{(n-1)}(i + 1, j) - u_x^{(n-1)}(i - 1, j) + u_y^{(n-1)}(i, j + 1) - u_y^{(n-1)}(i, j - 1) \right]. \tag{9}$$

The time step Δt must be small enough to ensure stability of the algorithm[13]:

$$\Delta t \le \frac{1}{c} \left(\frac{1}{\Delta x^2} + \frac{1}{\Delta y^2} \right)^{-\frac{1}{2}} = \frac{\delta}{\sqrt{2}\, c}, \qquad \text{(for two-dimension)} \tag{10}$$

In electromagnetism, a staggered lattice structure is normally used so that **E** and **H** are evaluated at interleaved lattice points in the space. This is appropriate for the FDTD representation of many EM problems. The aim of the present work is to establish a framework for our future studies of scattering from objects with realistic boundaries. In these cases, both p and **u** will often appear concurrently in boundary condition expressions. Therefore we choose a non-staggered lattice structure so that both field parameters are evaluated at the same lattice points. However, staggered lattice structures may also be useful for some acoustic applications.

Eqs. (7) – (9) provide explicit recurrence relations between p and **u**. The present p value can be computed from the p value of the same lattice point two time-steps earlier, together with the **u** values of the neighboring points one time-step earlier. The **u** values are computed in a similar way. The computer program can be written to update **u** and p alternately without solving any system of simultaneous equations.

B. Boundary conditions

The motivation of this study is to investigate back scattering of objects with complex shapes and realistic surface properties. Other approaches such as the geometrical theory of diffraction (GTD) are usually difficult to use for these applications. FDTD, on the other hand, solves the basic equations directly in the time domain, therefore is potentially advantageous in dealing with arbitrary shapes and surface impedances provided a suitable discrete form of the boundary conditions can be found. In the this work, however, we only study objects with different shapes and ideal impedance conditions.

Consider incident sound waves in the water propagated toward a solid object. In ideal cases, the surface may be either infinitely soft (pressure released surface), or infinitely rigid where the normal particle velocity must be zero. Since analytical solutions exist for some objects of canonical shapes with ideal boundary conditions, these cases are important for verification of the FDTD algorithm.

On an infinitely soft boundary, the sound pressure is set to zero in each recurrence cycle.

$$p^{(n)}(i, j) = 0, \qquad \text{(on boundary)}. \tag{11}$$

The particle velocity is then calculated to satisfy the motion equation.

For a harmonic time dependence, the normal particle velocity on the surface is proportional to the normal component of the pressure gradient. Therefore in the infinitely rigid case, p satisfies the following:

$$\frac{\partial p}{\partial x} \cos \alpha + \frac{\partial p}{\partial y} \sin \alpha = 0, \tag{12}$$

where α is the angle between the surface normal and the horizontal axis. Substituting the first-order difference expressions, Eqs. (7) – (9), into Eq. (12), and assuming that (i, j) is a boundary point, and (i-1, j) and (i, j-1) are within the water, the following relation is obtained:

$$p^{(n)}(i,\,j) \;=\; \frac{p^{(n)}(i\,-\,1,\,j)\cos\alpha(i,\,j) \;+\; p^{(n)}(i,\,j\,-\,1)\sin\alpha(i,\,j)}{\cos\alpha(i,\,j) \;+\; \sin\alpha(i,\,j)} \;. \tag{13}$$

It is important to ensure the availability of every p value on the right side of Eq. (13). Since (i+1, j) and/or (i, j+1) may be inside the solid object, biased differences are used here instead of central differences. For other boundary orientations, Eq. (13) should be modified accordingly. For example, if (i+1, j) and (i, j-1) are within the water, the following variation should be used.

$$p^{(n)}(i,\,j) \;=\; \frac{p^{(n)}(i\,+\,1,\,j)\cos\alpha(i,\,j) \;-\; p^{(n)}(i,\,j\,-\,1)\sin\alpha(i,\,j)}{\cos\alpha(i,\,j) \;-\; \sin\alpha(i,\,j)} \;. \tag{13a}$$

Of the two components of **u**, u_x and u_y , one can be calculated from the recurrence relation, using biased rather than central differences, and the other should be calculated from the following constraint:

$$u_x^{(n)}(i,\,j)\cos\alpha(i,\,j) \;+\; u_y^{(n)}(i,\,j)\sin\alpha(i,\,j) \;=\; 0 \;. \tag{14}$$

C. Absorbing boundary conditions

The computer modeling of wave propagation is only feasible in a finite spatial region. For scattering applications, this region should contain all the scatterers. The outer boundary of the region is assumed to be convex. The incident waves enter the region from outside, while the scattered waves can only travel outward at the truncating boundary and never come back. In other words, the outer boundary should be completely absorbent to the scattered waves, hence the term *absorbing boundary condition* (ABC).

Absorbing boundary conditions are an important research topic in the FDTD applications, and a number of approaches have been proposed[14,15,16]. The popular first-order ABC proposed by Mur is used in the present work. The second-order Mur's ABC may provide better results, but will require considerably more computer time and storage. Our recent studies on finding more accurate and numerically efficient absorbing boundary conditions for the underwater acoustics applications have resulted in a new method termed the least square (LS) ABC, described in a separate paper[17].

Figure 2 shows the geometry of the numerical model, where the object is a circular cylinder with a radius of R_0, and centered at the center of the rectangular region. The cylinder is insonified by a plane incident wave from the left. A Cartesian coordinate system is chosen as shown. The first-order Mur's ABC is based on the statement that, at the boundary x = 0, there are only scattered waves traveling in the negative x-direction:

$$\left[\frac{\partial f}{\partial x} \;-\; \frac{1}{c}\,\frac{\partial f}{\partial t}\right]_{x=0} \;=\; 0 \;. \tag{15}$$

The field parameter f in this equation may be p, u_x or u_y. This leads to a difference expression that can be used in the FDTD algorithm:

$$f^{(n)}(i\,,\,j) = f^{(n-1)}(i+1\,,\,j) + \frac{c\Delta t - \delta}{c\Delta t + \delta}\Big[f^{(n)}(i+1\,,\,j) - f^{(n-1)}(i\,,\,j)\Big] \;. \tag{16}$$

As in the case of boundary conditions, biased differences are used because the field values outside the region are not available. At the opposite boundary $x = x_1$ the following expression should be used instead:

$$f^{(n)}(i\,,\,j) = f^{(n-1)}(i-1\,,\,j) + \frac{c\Delta t - \delta}{c\Delta t + \delta}\Big[f^{(n)}(i-1\,,\,j) - f^{(n-1)}(i\,,\,j)\Big] \;. \tag{17}$$

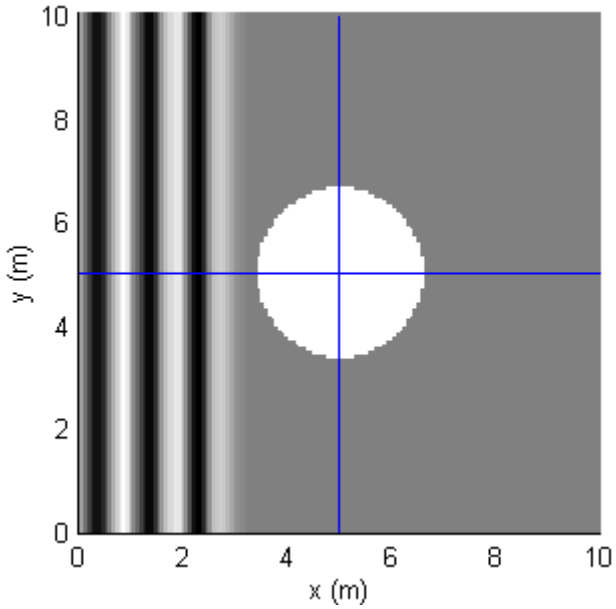

Figure 2 Plane wave is propagated in the positive *x*-direction, and about to hit a cylinder. The wavelength is 1m. The radius of the cylinder is 1.6m. The gray scale image visualizes the instantaneous pressure distribution obtained by time-stepping using FDTD with a grid size $\delta=\lambda/15$.

II. CONSIDERATIONS IN NUMERICAL COMPUTATIONS

A. General procedure

The FDTD algorithm is first applied to a classical case in which an ideally soft or ideally rigid cylinder is insonified by a plane incident wave. Figure 2 shows that a plane wave enters the region from the left, and is about to hit the object. The instantaneous pressure values of the plane wave are visualized by different gray levels, with the intermediate gray shade representing zero, and the darker and brighter shades representing negative and positive excursions respectively. The total near-field distribution is obtained by time-stepping the wave field within the rectangular region. After the object is fully insonified by the incident wave, and a steady-state is established in the areas of concern, the incident wave is subtracted from the total field, yielding a distribution of the scattered wave in the near-field. A near-field to far-field transformation procedure is then performed to derive the far-field directional pattern of the scattered waves.

The directional pattern obtained can be compared with the theoretical result that is a solution to the wave equation using the method of separation of variables in a polar coordinate system. When the cylinder is absolutely rigid, the theoretical far-field directional pattern of the pressure is given by[18]

$$\Psi_s(\phi) = \sum_{m=0}^{\infty} \varepsilon_m \sin(\gamma_m) e^{-i\gamma_m} \cos(m\phi) , \tag{18}$$

where λ_ms are the roots of the following transcendental equations:

$$\tan\gamma_0 = -\frac{J_1(ka)}{N_1(ka)} , \tag{19}$$

$$\tan\gamma_m = \frac{J_{m-1}(ka) - J_{m+1}(ka)}{N_{m+1}(ka) - N_{m-1}(ka)} , \qquad m > 0 . \tag{20}$$

In studying the directivity of the scattered waves, a polar coordinate system is used. Here ϕ is the directional angle ($\phi = 0$ corresponds to the direction of the plane wave propagation), k ($=\omega/c$) is the wave number, a is the radius of the cylinder, $\varepsilon_0 = 1$, and $\varepsilon_m = 2$ for $m > 0$.

Similarly, for an absolutely soft cylinder, the directional pattern is

$$\Psi_s(\phi) = \sum_{m=0}^{\infty} \varepsilon_m \cos(m\phi) \frac{J_m(ka)}{H_m^{(1)}(ka)} . \tag{21}$$

In scattering problems, an important consideration is to separate the incident and scattered waves properly. A method of dividing the lattice into total-field and scattered-field regions has been proposed[5]. This ensures natural satisfaction of the boundary conditions on the object surface, as well as provides a well-defined scattered-wave field permitting a near-field to far-field transformation in RCS studies. The present work, however, employs an alternative method. In addition to the total field computed in the whole region, the incident wave is computed using FDTD separately with the object removed. Subtracting the incident wave from the total field gives the scattered near-field. For a plane incident wave, the FDTD recurrence can be carried out in one dimension; therefore the additional computation needed is only a fraction of the total. On the truncating boundary, the ABCs are applied to both the incident and scattered waves. This method is easier to implement as it avoids extra treatments on the so-called connecting surfaces introduced in the proposed dual-region approach. Care must be taken though in identifying specific time instances of various components of the field when applying Mur's ABC at the outer boundary.

B. Near-field to far-field transformation

The far-field directional pattern of the scattered waves can be derived from the near-field distribution using Kirchhoff-Helmholtz integration[19] or the Fourier transform method[20]. In this paper, we use the Fourier transform approach. In a polar coordinate system, the sound pressure can be expanded into a series of cylindrical harmonics:

$$p(r,\phi) = \sum_{n=-\infty}^{\infty} a_n H_n^{(1)}(kr) e^{jn\phi}, \qquad -\pi \le \phi < \pi, \tag{22}$$

The Hankel functions of the first kind are used since the scattered waves are divergent. Taking N samples within $-\pi \le \phi < \pi$, with intervals $\delta\phi = 2\pi/N$, a discrete form is obtained:

$$p(r,l) = \sum_{n=-N/2}^{N/2-1} a_n H_n^{(1)}(kr) e^{jnl\delta\phi}, \qquad l = -\frac{N}{2},\ldots,-1,\ 0,\ 1,\ldots,\frac{N}{2}-1, \tag{23}$$

assuming that N is an even number. The interval $\delta\phi$ should be sufficiently small to provide a proper sampling. The truncation of the sum is permissible as our computations show that a_ns are significantly different from zero only for $|n| < 20$. These numerical experiments also show that an adequate angular resolution can be achieved when $N \ge 128$. Evaluate $p(r,\phi)$ on a circle with a radius r_0 that encloses all the scatterers:

$$p(r_0,l) = \sum_{n=-N/2}^{N/2-1} a_n H_n^{(1)}(kr_0) e^{jnl\delta\phi}, \qquad l = -\frac{N}{2},\ldots,-1,\ 0,\ 1,\ldots,\frac{N}{2}-1. \tag{24}$$

In the computation, a cubic spline interpolation is performed to obtain the uniformly angular-spaced samples $p(r_0, l)$ from the p values on the rectangular lattice, obtained from the FDTD recurrence. Thus the following discrete Fourier pair is obtained:

$$P(n) = \sum_{l=-N/2}^{N/2-1} p(r_0,l) e^{-jnl\delta\phi}, \qquad n = -\frac{N}{2},\ldots,-1,\ 0,\ 1,\ldots,\frac{N}{2}-1. \tag{25}$$

$$p(r_0,l) = \frac{1}{N} \sum_{n=-N/2}^{N/2-1} P(n) e^{jnl\delta\phi}, \qquad l = -\frac{N}{2},\ldots,-1,\ 0,\ 1,\ldots,\frac{N}{2}-1. \tag{26}$$

From Eqs. (24) and (26), the coefficients a_ns are found:

$$a_n = \frac{P(n)}{N H_n^{(1)}(kr_0)}, \qquad n = -\frac{N}{2},\ldots,-1,\ 0,\ 1,\ldots,\frac{N}{2}-1. \tag{27}$$

In the far field where $kr >> 1$, Eq. (23) can be simplified by using the asymptotic form of the Hankel functions:

$$p(r,l) = \sqrt{\frac{2}{\pi kr}}\, e^{jkr} \sum_{n=-N/2}^{N/2-1} a_n j^{n+2} e^{jnl\delta\phi}, \qquad l = -\frac{N}{2},\ldots,-1,\ 0,\ 1,\ldots,\frac{N}{2}-1. \tag{28}$$

It now becomes clear that the far-field directional pattern is the inverse Fourier transform of the data sequence $a_n j^n$:

$$\Psi(l) = \sum_{n=-N/2}^{N/2-1} a_n j^n e^{jnl\delta\phi}, \qquad l = -\frac{N}{2}, \ldots, -1, \ 0, \ 1, \ldots, \frac{N}{2} - 1. \tag{29}$$

III. COMPUTER EXPERIMENT RESULTS

A. Scattering from ideal cylinders

Figure 3 shows the scattering of an ideally soft circular cylinder insonified by a plane wave, where (a) and (b) are the instantaneous pressure distribution of the total and scattered field around the cylinder respectively. The geometry is the same as shown in Figure 2. The plus signs in both plots indicate the location of the incident wave front. A frequency f_0=1500Hz, therefore λ = 1m, was used. (The same frequency was used for all the numerical experiments in this paper.) The cylinder diameter R_0 = 1.6m. The size of the region was 10×10m, and a step size $\delta = \lambda/15$ was chosen. It is clear from the plots that the scattered waves were emitted from the object, and interfered with the incident plane wave.

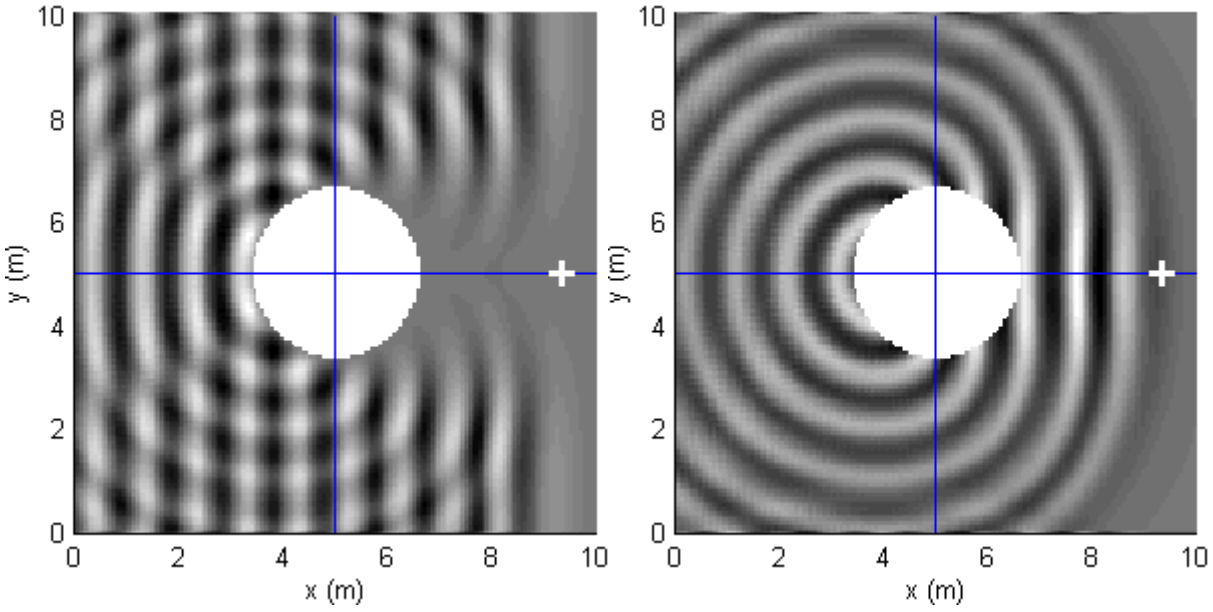

Figure 3 Scattering of a soft cylinder with plane wave incidence. Distribution of pressure magnitude: (a) the total field, and (b) the scattered wave. The geometry and wave parameters are the same as in Figure 2.

Figure 4 shows the far-field directional pattern of the scattered pressure magnitude. Patterns of sound pressure rather than intensity are presented in order to give a better view of the back scattering. The solid curve is obtained by using the Fourier transform method from the near-field pressure distribution shown in Figure 3(b). A 256-point FFT was used in the computation. The main lobe in the plot indicates that the strongest scattering was in the forward direction. It is in opposite phase with the incident wave, therefore canceling the incident wave to yield a shadow region. This pattern is compared with the dashed curve that is a theoretical result computed from Eq. (21). The good agreement between the two curves provides a verification of the FDTD algorithm.

The near-field distributions of the total and scattered sound pressure around an ideally rigid cylinder are presented in Figure 5. Figure 6 gives the comparison of the far-field directional patterns of the FDTD and the theoretical methods. All the wave parameters and the geometry are the same as the soft case.

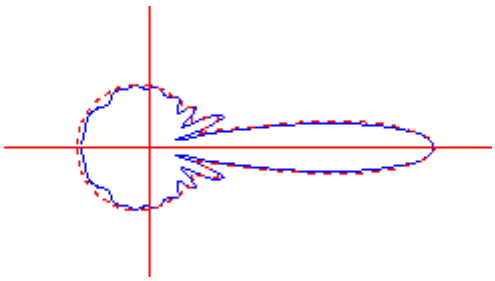

Figure 4 Far-field directional pattern (solid curve) of the scattered wave from a soft cylinder derived from the near field shown in Figure 3, compared with the dashed curve based on an exact solution.

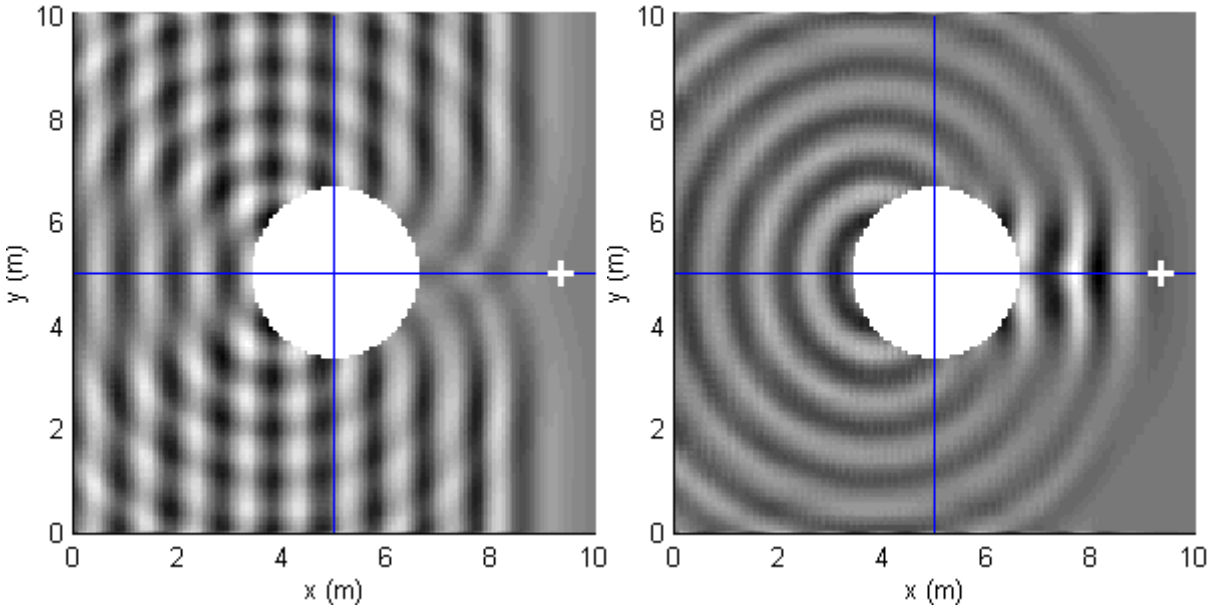

(a) (b)

Figure 5 Scattering of a rigid cylinder. (a) Total field. (b) Scattered wave.

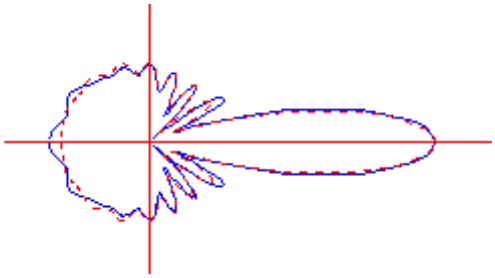

Figure 6 Far-field directional pattern of the scattered wave from a rigid cylinder (solid). The dashed curve is based on an exact solution.

B. Scattering from a rectangular cylinder

Figure 7 shows the near-field distributions of the total and scattered sound pressure around a soft rectangular cylinder, 1.5×3m in size. The cylinder was placed in the field such that the angle between one side and the horizontal axis was 45°. The step size used was $\delta = \lambda/12$. Figure 8 presents two directional patterns. The solid curve corresponds to the case shown in Figure 7, whereas the dashed curve is obtained with the rectangle rotated clockwise by 15°. Besides a mainlobe in the forward direction, there are two additional major lobes in each case. These clearly correspond to the specular reflection from the insonified sides of the object. This example shows that the FDTD method is readily applicable to various geometric shapes other than those manageable by most exact or asymptotic approaches.

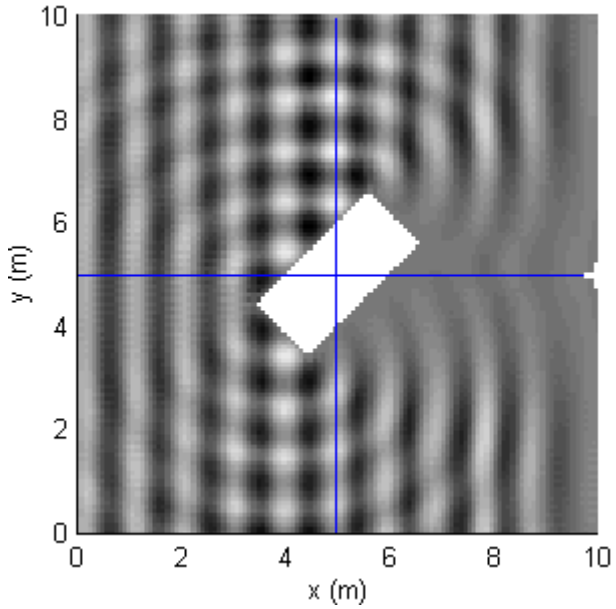

Figure 7 Scattering of a rectangular cylinder: the total field. λ=1m, $\delta=\lambda/12$. The lengths of the sides are 1.5m and 3m respectively. The angle between one side and the x-axis is 45°.

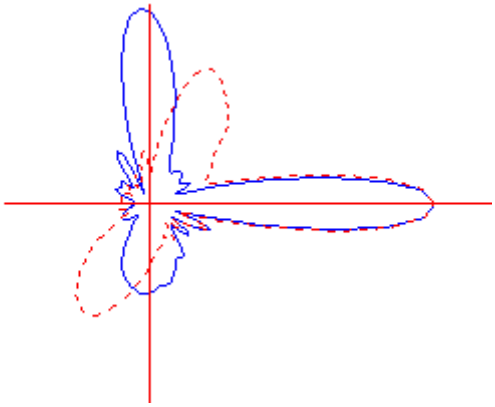

Figure 8 Far-field directional pattern (solid) derived from the near-field shown in Figure 7. The main lobe in the forward direction corresponds to the geometrical shadow; and the other two major lobes in 90° and 270° directions correspond to specular reflection. The dashed curve is obtained with the rectangle rotated clockwise by 15°, therefore the specular reflections appear in 60° and 240°.

C. Edge diffraction by wedges

The FDTD algorithm has been applied to a wedge diffraction problem where both a rigorous solution and an asymptotic solution obtained by using GTD are available.

An infinitely soft wedge with an interior angle equal to 21° was first used. Figure 9 shows the instantaneous pressure distribution around the diffracting edge, with a plane wave normally incident on the front surface. Evidently, the diffracted waves originate from the edge, and spread cylindrically. The step size used was $\delta = \lambda/12$. The magnitude of the sound pressure on a line behind the wedge, and 2λ from the front face as shown by the chained line in Figure 9, has been computed and plotted in Figure 10 (solid curve). The dashed curve in the plot is based on a rigorous solution in a form of an eigenfunction series obtained by solving the wave equation with separation of variables[21]:

$$p(r,\theta) = p_0 \sum_{n=0}^{\infty} \varepsilon_n e^{j\nu\pi/2} J_\nu(kr)\left\{\cos[\nu(\theta - \theta_0)] \mp \cos[(\nu(\theta + \theta_0)]\right\}, \qquad (30)$$

where the minus and plus signs correspond to soft and rigid boundaries respectively. ε_0=1/2, and ε_n =1 for n > 1. θ is measured from the front face of the wedge. θ_0 is the angle between the incident ray and the front face. The non-integer orders of Bessel functions are related with the wedge angle β:

$$\nu = \frac{n\pi}{2\pi - \beta} \quad , \qquad n = 0,\ 1,\ 2, \ldots \tag{31}$$

The FDTD result of diffraction from a rigid wedge with the same geometry is presented in Figures 11 and 12. From these plots one can see that, in the case of a rigid wedge, the plane incident wave in the upper region is less perturbed by the diffracted waves compared with the case of a soft wedge. More diffracted energy enters the shadow area of a rigid wedge than that of a soft wedge. This is in agreement with the statements found in an earlier study using GTD[21].

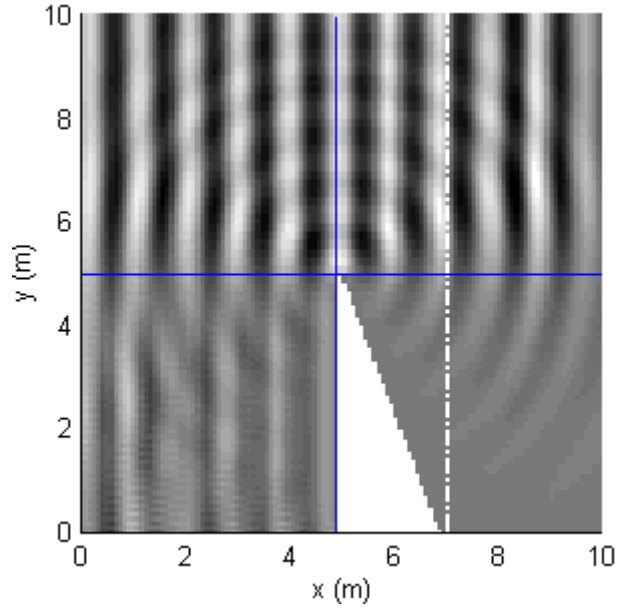

Figure 9 Diffraction by a soft wedge: the total field around the edge. λ=1m, δ=λ/12. The wedge angle is 21°. The incident direction is perpendicular to the front face. The pressure magnitude on the chained line is compared with the theoretical result, and shown in Figure 10.

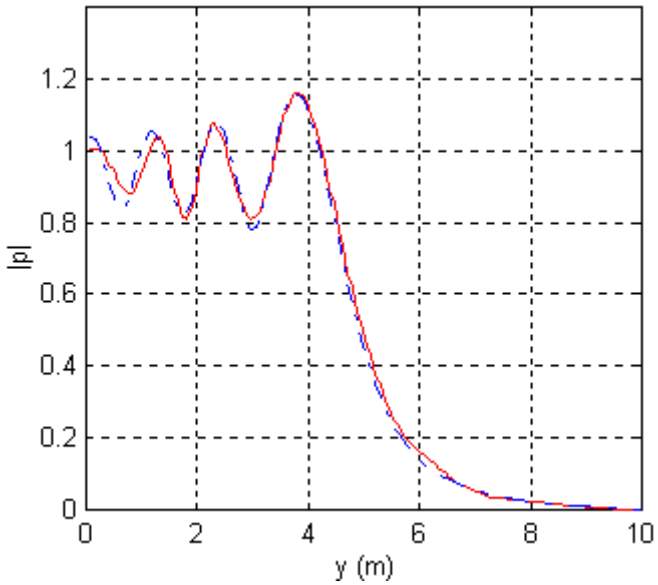

Figure 10 Distribution of the pressure magnitude along a line behind the soft wedge. The line and the front face are in parallel, and 2m apart (see Figure 9). The solid curve is the FDTD result, while the dashed curve is obtained from a rigorous solution.

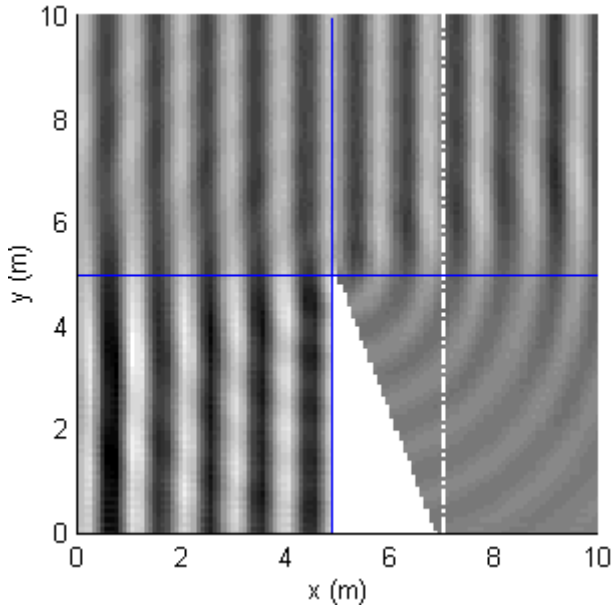

Figure 11 Diffraction by a rigid wedge. The geometry and wave parameters are the same as the soft case.

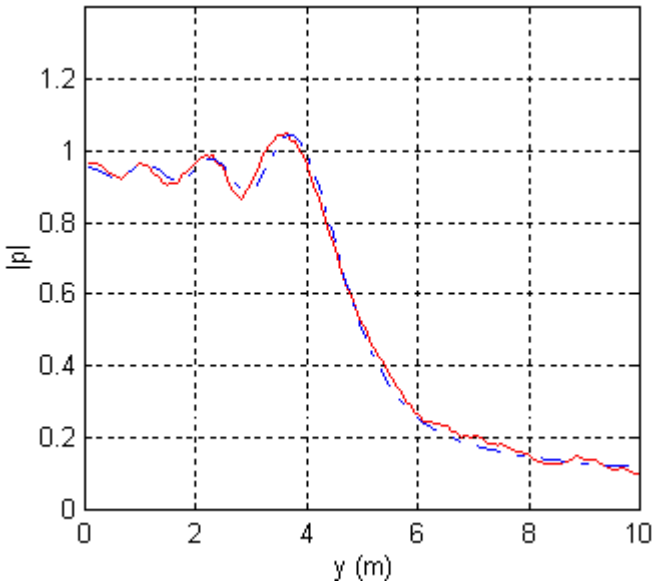

Figure 12 Distribution of the pressure magnitude along a line behind the rigid wedge. The FDTD result (solid) is compared with the rigorous solution (dashed).

IV. CONCLUSIONS

The finite-difference time-domain method has found a wide variety of applications in many spheres, electromagnetism in particular, due to its simple concept, manageable yet robust numerical algorithm, and high accuracy. In a hope of leading to solutions to some difficult scattering problems, an effort has been made to implement the FDTD method in underwater acoustics. In this paper, the recurrence relations between sound pressure and particle velocity are formulated, and the discrete form of the boundary conditions for infinitely soft and infinitely rigid objects is presented. The FDTD algorithm is applied to several scattering problems with ideal boundary conditions. Mur's first-order absorbing boundary conditions have been used in the computation. A field distribution around the scattering object is produced; and the far-field directional pattern is derived by a Fourier transform approach.

Steady-state, single frequency situations were assumed; and ideal scattering objects were used in this study in order to make comparisons with some known solutions. In the cases where such comparisons are possible, the agreement is remarkably good. This provides confidence in applying the method to various aspects of underwater acoustics.

The method is also well suited for broad-band transient problems[3] that is part of our present research interests. Implementations of the method to realistic scatterers with various boundary properties are currently under investigation as well. These will include both opaque and penetrable objects. The latter may be dissipative or elastic.

It is worth noting that treatments of acoustic problems including scattering using conformal mapping techniques have been reported[22]. This may provide a method to simplify the FDTD algorithm in dealing with objects with complicated shapes.

ACKNOWLEDGMENTS

This work is supported by National Natural Science Foundation of China. The author wishes to thank Professor Feng Shaosong of Shanghai Acoustics Laboratory, Professor Wang Zuomin of Tongji University, and Professor Zhu Beili of Shanghai Jiaotong University for their comments in the discussions over the near-field to far-field transformation.

1. K. S. Yee, "Numerical Solution of Initial Boundary Value Problems Involving Maxwell's Equations in Isotropic Media," *IEEE Trans. Antennas Propagat.*, **AP-14**, 302-307 (1966)
2. R. J. Luebbers, and J. Beggs, "FDTD Calculation of Wide-Band Antenna Gain and Efficiency," *IEEE Trans. Antenna Propagat.*, **AP-40**, 1403-1407 (1992)
3. J. G. Maloney, and G. S. Smith, " A Study of Transient Radiation from the Wu-King Resistive Monopole – FDTD Analysis and Experimental Measurements," *IEEE Trans. Antenna Propagat.*, **AP-41**, 668-676 (1993)
4. P. A. Tirkas, C. A. Balanis, M. P. Purchine, and G. C. Barber, "Finite-Difference Time-Domain Method for Electromagnetic Radiation, Interference, and Interaction with Complex Structures," *IEEE Trans. Electromagn. Compat*., **EMC-35**, 192-203 (1993)
5. A. Taflove, and K. R. Umashankar, "Review of FD-TD Numerical Modeling of Electromagnetic Wave Scattering and Radar Cross Section," *Proc. IEEE*, **77**, 682-699 (1989)
6. K. R. Kelly, R. M. Alford, S. Treitel, and R. W. Ward, "Application of Finite Difference Methods to Exploration Seismology," in *Proc. Roy. Irish Acad. Conf. on Numerical Analysis*, (Academic Press, London and New York, 1974), pp. 57-76
7. M. E. Dougherty, and R. A. Stephen, "Geoacoustic Scattering from Seafloor Features in the ROSE Area," *J. Acoust. Soc. Am*., **82**, 239-256 (1987)
8. W. F. Chang, and G. A. McMechan, "Absorbing Boundary Conditions for 3-D Acoustic and Elastic Finite-Difference Calculations," *Bull. Seism. Soc. Am*, **79**, 211-218 (1989)
9. P. J. Roache, *Computational Fluid Dynamics*, Hermosa Press, Albuquerque, N. M. (1972)
10. J. A. Clark, and M. A. Sartori, "Numerical Propagation of Spatially Distributed Acoustic Sources Using the Exterior Helmholtz Integral Equation," in *IEEE Sixth SP Workshop on Statistical Signal and Array Processing Conference Proceedings*, (New York, NY, Oct. 1992), 338-341
11. J. R. Fricke, "Acoustic Scattering from Elemental Arctic Ice," *J. Acoust. Soc. Am*., **93**, 1784-1796 (1993)
12. R. A. Stephen, "A Review of Finite Difference Methods for Seismo-Acoustic Problems at the Seafloor, " *Reviews of Geophysics*, **26**, 445-458 (1988)
13. A. Taflove, and M. E. Brodwin, "Numerical Solution of Steady-State Electromagnetic Scattering Problems Using the Time-Dependent Maxwell's Equations," *IEEE Trans. Microwave Theory Tech*., **MTT-23**, 623-630 (1975)
14. G. Mur, "Absorbing Boundary Conditions for the Finite-Difference Approximation of the Time-Domain EM Field Equations," *IEEE Trans. Electromagn. Compat*., **EMC-23**, 377-382 (1981)
15. J. Fang, and K. K. Mei, "A Super-Absorbing Boundary Algorithm for Solving Electromagnetic Problems by Time-Domain Finite Difference Method," in *Proc. 1988 IEEE AP-S Int. Symp*. (Syracuse, NY, June 1988), pp. 472-475
16. C. J. Railton, and E. M. Daniel, "Comparison of the Effect of Discretisation on Absorbing Boundary Algorithms in the Finite Difference Time Domain Method," *Electronic Letters*, **628**, 1891-1893 (1992)
17. S. Wang, "An Efficient Absorbing Boundary for Finite-Difference Time-Domain Field Modeling in Acoustics, " submitted to *Acta Acustica*
18. P. M. Morse, *Vibration and Sound*, (American Institute of Physics, 1983), Chap. 7, pp. 347-350
19. R. J. Bobber, *Underwater Electroacoustic Measurements*, (Naval Research Laboratory, Washington, D.C., 1970), Chap. 4, pp. 193-195
20. E. V. Jull, *Aperture Antennas and Diffraction Theory*, (Peter Peregrinus, London, 1981), Chap. 4, pp. 38-41
21. S. Wang, "The Diffracted Acoustic Field around a Wedge," *Chin. J. Acoust*., **3**, 121-132 (1984) (Chinese edition: *Acta Acustica*, **10**, 247-256 (1985))
22. R. Schinzinger, and P. A. A. Laura, *Conformal Mapping: Methods and Application*, Elsevier, pp. 339-340